RSC Advances

PAPER

View Article Online
View Journal | View Issue

Cite this: *RSC Adv.*, 2019, **9**, 40424

Electrocatalytic water oxidation by a Ni(II) salophen-type complex†

Mehri Aligholivand,[a] Zohreh Shaghaghi, *[a] Rahman Bikas [b] and Anna Kozakiewicz [c]

A new mononuclear Ni(II) complex, NiL (**1**), was synthesized from the reaction of $Ni(OAc)_2 \cdot 4H_2O$ and salophen-type N_2O_2-donor ligand, H_2L (where H_2L = 2,2′-((1*E*,1′*E*)-((4-chloro-5-methyl-1,2-phenylene) bis(azanylylidene))bis(methanylylidene))diphenol), in ethanol. The obtained complex was characterized by elemental analysis, spectroscopic techniques and single crystal X-ray analysis. The complex was studied as a water oxidizing catalyst and its electrocatalytic activity in the water oxidation reaction was tested in 0.5 M of borate buffer at pH = 3, 7 and 11 in a typical three-electrode setup with a carbon paste electrode modified by complex **1** as a working electrode. The linear sweep voltammetry (LSV) curves indicated that complex **1** has a much superior activity and only needs 21 mV *vs.* Ag/AgCl overvoltage to reach a geometrical catalytic current density of 2.0 mA cm^{-2} at pH = 11. The onset potential decreased from 1.15 V to 0.67 V *vs.* Ag/AgCl with an increase of pH from 3 to 13 under a constant current density of 1.0 mA cm^{-2}. Then, to determine the true catalyst for the water oxidation reaction in the presence of complex **1** at pH = 3, 7 and 11, cyclic voltammetry was also performed. The continuous CVs for complex **1** at neutral and alkaline solutions showed significant progress for the water oxidation reaction. In addition, the amperometry tests exhibited excellent stability and high constant current density for water oxidation by CPE-complex **1** under electrochemical conditions at pH = 11 and 7. Although X-ray powder diffraction analysis did not show a pure and crystalline structure for NiO_x, the scanning electron microscopy images showed that nickel oxide at pH = 11 and nickel oxide or other Ni-based compounds at pH = 7 are true water oxidizing catalysts on the surface of a CPE electrode. Moreover at pH = 3, no clear water oxidation or NiO_x formation was observed.

Received 20th October 2019
Accepted 28th November 2019

DOI: 10.1039/c9ra08585h

rsc.li/rsc-advances

Introduction

The lack of fossil fuels and many environmental problems such as increasing greenhouse gases, release of pollutants *etc.*, which are produced in the burning of these fuels, reveals the need for new and renewable energy resources.[1] For this reason, hydrogen is considered as one of the most important carriers of energy because of its renewable, cheap and clean nature. In recent decades, many efforts have been made to explore reliable methods for the production of hydrogen and oxygen by oxygen evolution and hydrogen evolution reactions (OER and HER) through water splitting by various types of homogenous and heterogeneous catalysts.[2] Homogenous water oxidation catalysts are useful in the examination of reaction mechanisms and identification of the active intermediates which will give an opportunity for the precise designing of catalysts, while water insoluble catalysts can allow for easier post-reaction separation and recyclability.[3]

Water splitting can be divided two half-reactions: proton reduction ($2H^+ + 2e \rightarrow H_2$) and water oxidation ($2H_2O \rightarrow 4H^+ + O_2 + 4e$). Water oxidation is a slow electrochemical reaction with a high potential of about 1.23 eV. The oxidation of water to oxygen is a $4e/4H^+$ process which requires a large overpotential for the O–O bond formation. So, water oxidation has high activation energy and this matter is considered as a limiting step in water splitting.[4] On the other hand, at this high voltage the remaining chemical compounds in water, including some ions such as chloride and sulphate, can also be oxidized. Therefore, the design of suitable catalysts to reduce water oxidation potential seems essential. Due to this, the development of stable and cheap water oxidation catalysts is an important challenge for the design of water splitting systems.[5] Recently, molecular water oxidation catalysts based on first row transition metals have attracted considerable attention because of their low cost, high

[a]*Coordination Chemistry Research Laboratory, Department of Chemistry, Faculty of Science, Azarbaijan Shahid Madani University, P.O. Box 83714-161, Tabriz, Iran. E-mail: shaghaghi@azaruniv.ac.ir; zsh024@gmail.com*

[b]*Department of Chemistry, Faculty of Science, Imam Khomeini International University, 34148-96818, Qazvin, Iran*

[c]*Department of Biomedical and Polymer Chemistry, Faculty of Chemistry, Nicolaus Copernicus University in Torun, 87-100 Torun, Poland*

† Electronic supplementary information (ESI) available. CCDC 1954803. For ESI and crystallographic data in CIF or other electronic format see DOI: 10.1039/c9ra08585h

abundance and low environmental effects.[6] Previous studies indicate that the coordination compounds containing manganese,[7] iron,[8] nickel,[9] cobalt[10] and copper ions[11] can oxidize water under different conditions. Among water oxidation catalysts based on 3d transition metals, Ni-containing materials have attracted particular attention due to their good water oxidation potential and high oxidation power.[12] In fact, Ni-containing mixed-metal oxides or hydroxides are one of the efficient water oxidation catalysts.[13] Ni complexes are often investigated as heterogeneous water oxidation catalysts and few reports are available about nickel complexes as homogenous catalysts. For example, Ding groups have been reported mononuclear Ni(II) complexes containing tetradentate N_4^-, N_3O^- or N_2O-donor ligands ($C_{12}H_{10}N_4NiO_4\cdot 4H_2O$, $C_{11}H_7N_3NiO_5\cdot 5H_2O$ and $C_{10}H_4N_2NiO_6\cdot 6H_2O$). They found that $C_{12}H_{10}N_4NiO_4\cdot 4H_2O$ can act as a homogenous molecular catalyst, but two other complexes decompose to NiO_x nanoparticles and in fact act as precatalyst for electrochemical water oxidation.[14] Najafpour and co-workers presented a tetranuclear Ni(II) complex with bis-[(*E*)-*N*,*N*′-(1-(pyridin-2-yl)ethylidene)]carbohydrazide which catalyzes the oxidation of water. They realized that under water oxidation condition in the presence of this complex, nickel oxide or free Ni(II) ions oxidize water.[15] Feizi *et al.*[16] investigated the activity of *N*,*N*′-bis-(salicylidene)ethylenediamino nickel(II) at three different pH. It was revealed that the complex is very active for water oxidation at a high pH. Zhang *et al.*[17] designed a Ni(II) complex [Ni(*meso*-L)] $(ClO_4)_2$ (L = 5,5,7,12,12,14-hexamethyl-1,4,8,11-tetraazacyclotetradecane) as a homogenous electrocatalyst for water oxidation which could act at neutral pH and low overpotential in phosphate buffer. Barros *et al.*[18] investigated water oxidation activity of a family of Ni(II) complexes containing oxamidate anionic type of ligands in basic pH. They found that during the water oxidation process, the degradation of the molecular species generates a NiO_x layer which is stable and active as electrocatalyst. Han *et al.*[19] reported the water soluble Ni(II) complex of *meso*-tetrakis(4-*N*-methylpyridyl)porphyrin which could electrocatalyze water oxidation in neutral aqueous solution with the onset of the catalytic wave appearing at ~1.0 V (*vs.* NHE). Sun groups designed a Ni-Py5 [Py5 = 2,6-bis(1,1-bis(2-pyridyl)ethyl)pyridine)] complex which could act as a homogenous electrocatalyst for oxidizing water in aqueous phosphate buffer solutions.[20] Hill's group presented a nickel-containing polyoxometalate $[Ni_5(OH)_6(H_2O)_3(Si_2W_{18}O_{66})]^{12-}$ which oxidized water in the presence of $[Ru(bpy)_3]^{3+}$. The evidences showed that this catalyst remains molecular throughout and does not form a nickel hydroxide or nickel oxide under the conditions of catalytic water oxidation reaction.[21] According to the literature,[15,16,22] free Ni(II) ions or Ni oxides can catalyze the water oxidation reaction at low concentration and high pH. There are always some key questions in this regard: "do the Ni complexes molecularly catalyze the oxidation of water?" or "whether the complexes decompose under water oxidation or convert to Ni oxide which catalyzes the water oxidation reaction?" and most importantly, "which is the true catalyst for water oxidation? Metal complex, impurity or decomposed complex?" Determination of this is not easy, and thus leads to a great deal of encouragement by researchers for the preparation of new electrocatalysts of nickel complexes. Here, we reported synthesis and crystal structure of a new Ni(II) complex with salophen-type ligand, (H_2L = (2,2′-((1*E*,1′*E*)-((4-chloro-5-methyl-1,2-phenylene)bis(azanylylidene)) bis(methanylylidene))diphenol). We also investigated the application of this complex for electrochemical water oxidation at pH = 3, 7 and 11. By using various methods we showed that the designed Ni(II) complex is an efficient electrocatalyst for water oxidation in neutral and basic solutions. Researches show that nickel complexes exhibit high activity for water oxidation reaction in basic or high pH conditions in phosphate and borate buffers.[18,23] There are few reports of nickel complexes which act as active electrocatalyst for the oxidation of water in neutral pH, and most of them are homogeneous catalysts of nickel complexes in the presence of phosphate buffer.[17,19,24] A unique feature of this work compared to previous works is the design of a new heterogeneous electrocatalyst from nickel complexes that can catalyze water oxidation reaction in neutral solutions as well as basic solutions.

Results and discussion

Synthesis and characterization

The NiL (**1**) complex is prepared by the reaction of the salophen-type Schiff-base ligand, H_2L (2,2′-((1*E*,1′*E*)-((4-chloro-5-methyl-1,2-phenylene)bis (azanylylidene))bis(methanylylidene))diphenol) with $Ni(OAc)_2\cdot 4H_2O$ and characterized by single crystal X-ray analysis and spectroscopic techniques as well as elemental analysis. The molecular structure of complex **1** with atom numbering scheme is shown in Fig. 1 and selected bond lengths and angles around the Ni atom are summarized in Table 1. Structural studies indicated that **1** is a mononuclear Ni(II) complex which crystallizes in $P2_1/c$ space group of monoclinic system. Complex **1** is a neutral coordination compound and the Ni(II) ion has a square planar *cis*-NiN_2O_2 coordination environment. This coordination environment is generated by coordination of two phenolate oxygen and two azomethine nitrogen atoms from the salophen-type N_2O_2-donor ligand. The Ni–N and Ni–O bond lengths are in the normal range observed for Ni(II) complexes. Due to the coordination of ligand to metal ion a five membered ring (NiN_2C_2) and two six membered heterocyclic rings containing Ni, N and O atoms (NiC_3NO) have been generated in the structure of complex. There is a strong Ni⋯Ni interaction in the crystal structure of complex **1** with Ni⋯Ni distance of 3.264(2) Å (see Fig. 2). Moreover, there are several π⋯π stacking interactions between the phenyl ring and heterocyclic rings containing Ni(II) ion which are shown in Fig. 3. The crystal structure of complex is further stabilized by intermolecular C–H⋯O and C–H⋯Cl interactions (see Fig. S1 and Table S1†).

Ni complex **1** is further characterized by FT-IR and ^{1}H NMR spectroscopy. FT-IR spectroscopy data shows that after complexation with nickel, the absorption of imine vibration shifts from 1614 cm^{-1} for the ligand to shorter wavenumbers about 6 cm^{-1} for the complex. This suggests the coordination of the electron pair of nitrogen atoms of imine groups to the metal ion center.[25,26] Also, the disappearance of the broad absorption band at 3447 cm^{-1} indicates that the phenolic hydroxyl groups

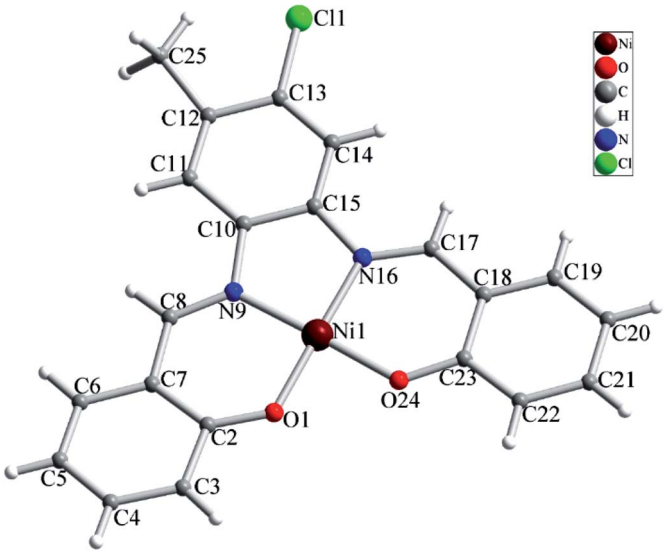

Fig. 1 Molecular structure of complex **1** with atom numbering scheme.

Table 1 Selected bond lengths and angles in the crystal structure of complex **1**

Bond	Length/Å	Bond	Angle/°
Ni1–O24	1.817(8)	O24–Ni1–O1	83.7(3)
Ni1–O1	1.834(7)	O24–Ni1–N9	178.2(4)
Ni1–N9	1.837(9)	O1–Ni1–N9	94.5(4)
Ni1–N16	1.849(9)	O24–Ni1–N16	95.6(4)
C8–N9	1.298(14)	O1–Ni1–N16	178.9(4)
N16–C17	1.302(14)	N9–Ni1–N16	86.1(4)

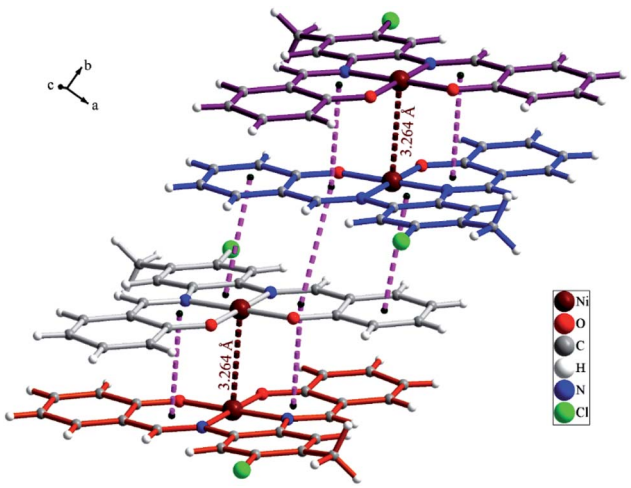

Fig. 2 Ni···Ni and π···π interactions in the crystal structure of complex **1**.

are deprotonated when bound to the Ni(II) ion. In additional, the ν(M–O) and ν(M–N) are identified in the range of 449–595 cm^{-1}. Finally, the medium peaks about 752 cm^{-1} are related to chlorine (C–Cl) (Fig. S2†).

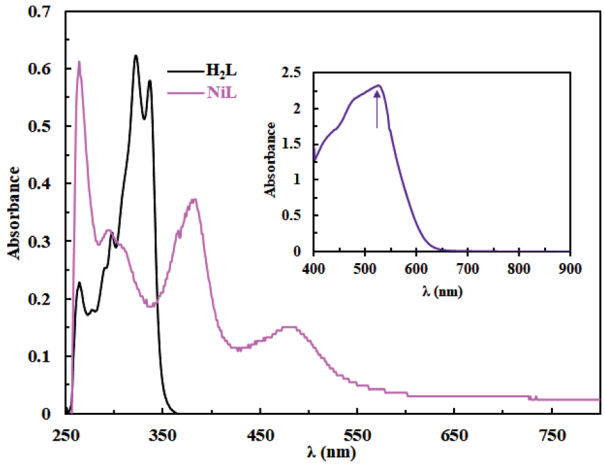

Fig. 3 UV/Vis spectra of H_2L and complex **1** in DMSO (3×10^{-5} M); inset: d → d transitions of complex **1** (10^{-3} M).

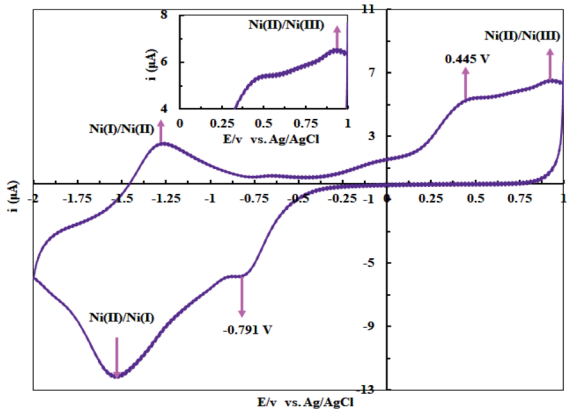

Fig. 4 The cyclic voltammogram of complex **1** (10^{-3} M) in DMSO solution containing 0.1 M $LiClO_4$ as a supporting electrolyte at room temperature in a potential rang of +1.0 to −2.0 V *vs.* Ag/AgCl at 50 mV s^{-1} potential scan rate.

In the ^{1}H NMR spectrum of the complex, the singlet resonances corresponding to the none-equivalent –OH protons, which are observed at 12.70 ppm and 12.77 ppm for the ligand, are disappear. This indicates that the phenolic hydroxyl groups are deprotonated when bound to a Ni(II) ion. Also, in comparison with the ligand, the imine proton resonances shift to downfield and appear at 9.02 ppm and 8.97 ppm which confirm the coordination of nitrogen atoms of imine groups to the Ni(II) center (in the ^{1}H NMR spectrum of the ligand, the two none-equivalent imine proton resonances are observed at 8.95 ppm and 8.99 ppm).[27,28] Moreover, the aromatic protons are observed at 6.73–8.32 ppm and the protons of $–CH_3$ group appear at 2.14 ppm (Fig. S3†).

The UV/Vis spectra of H_2L and complex **1** in DMSO solution (3×10^{-5} M) are shown in Fig. 3. The absorption spectra exhibit intense bands in the 258–337 nm region, which is attributed to the π → π* and n → π* intra-ligand transitions.[26] The intensity of n → π* transition decreases after complex formation which

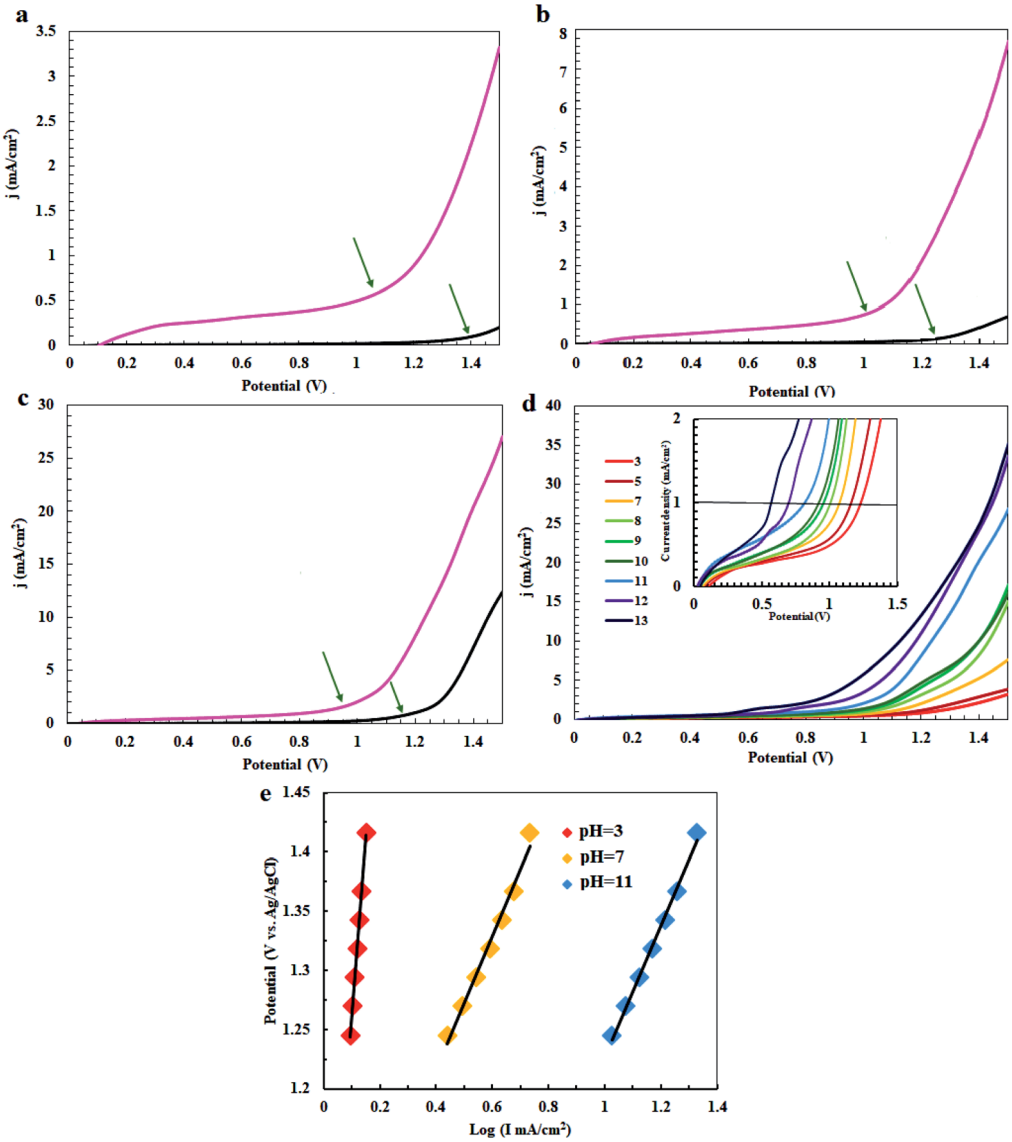

Fig. 5 Linear sweep voltammetry (LSV) curves of a fresh CPE (black) and CPE modified with complex **1** (pink) in buffer solution at pH = 3 (a), pH = 5 (b), pH = 11 (c), LSV curves for CPE-complex **1** at pH = 3–13 (d) and Tafel plots of CPE-complex **1** at pH = 3, 7 and 11 (e).

can be attributed to the coordination of the azomethine groups to the metal ion. For complex **1**, the absorption bands at 385 nm and 483 nm can be assigned to the L → M charge transfers transitions (LMCT).[26,29] It should be noted that d → d transition appears as a low intensity board absorption band at 531 nm. In addition, the thermal stability of the complex was investigated by thermogravimetric analysis (TGA) under N_2 atmosphere. The TGA plot of Ni(II) complex shows that the complex is stable up to 400 °C with a DTG_{max} = 410 °C and the highest weight loss occurs in the range of 590–800 °C which corresponds to the decomposition of the residue aromatic groups and the formation of metal oxide lattice (see Fig. S4†).

Electrochemistry and water oxidation

The +2 oxidation state is a common oxidation state for Ni complexes while the other oxidation states (like +1, +3 and +4) are rarely reported.[30] According to the literature,[31] Ni(II) salen complex (salen = *N*,*N*′-bis-(salicylidene)-1,2-ethyleneamine) shows Ni(II)/Ni(III) oxidation at +0.71 V *vs.* SCE and Ni(I)/Ni(II) oxidation at −1.61 V *vs.* SCE in DMSO. The Ni(II) complexes with salophen ligand (salophen = *N*,*N*′-bis-(salicylidene)-1,2-phenylenediamine) and its phenyl-substituted counterparts display chemically reversible Ni(II)/Ni(III) oxidation. Fig. 4 shows the voltammogram of complex **1** in DMSO solution (10^{-3} M) containing 0.1 M $LiClO_4$ as a supporting electrolyte at room temperature in a potential range of +1.00 to −2.00 V *vs.* Ag/AgCl at 50 mV s^{-1} potential scan rate (the glassy carbon, the Pt wire and the Ag/AgCl electrodes were used as working, counter and reference electrodes, respectively). Complex **1** exhibits a one electron oxidation at 0.934 V *vs.* Ag/AgCl which can be assigned to the Ni(II) → Ni(III) oxidation process. The anodic peak at −1.25 V and the cathodic peak at −1.51 V are attributed to the

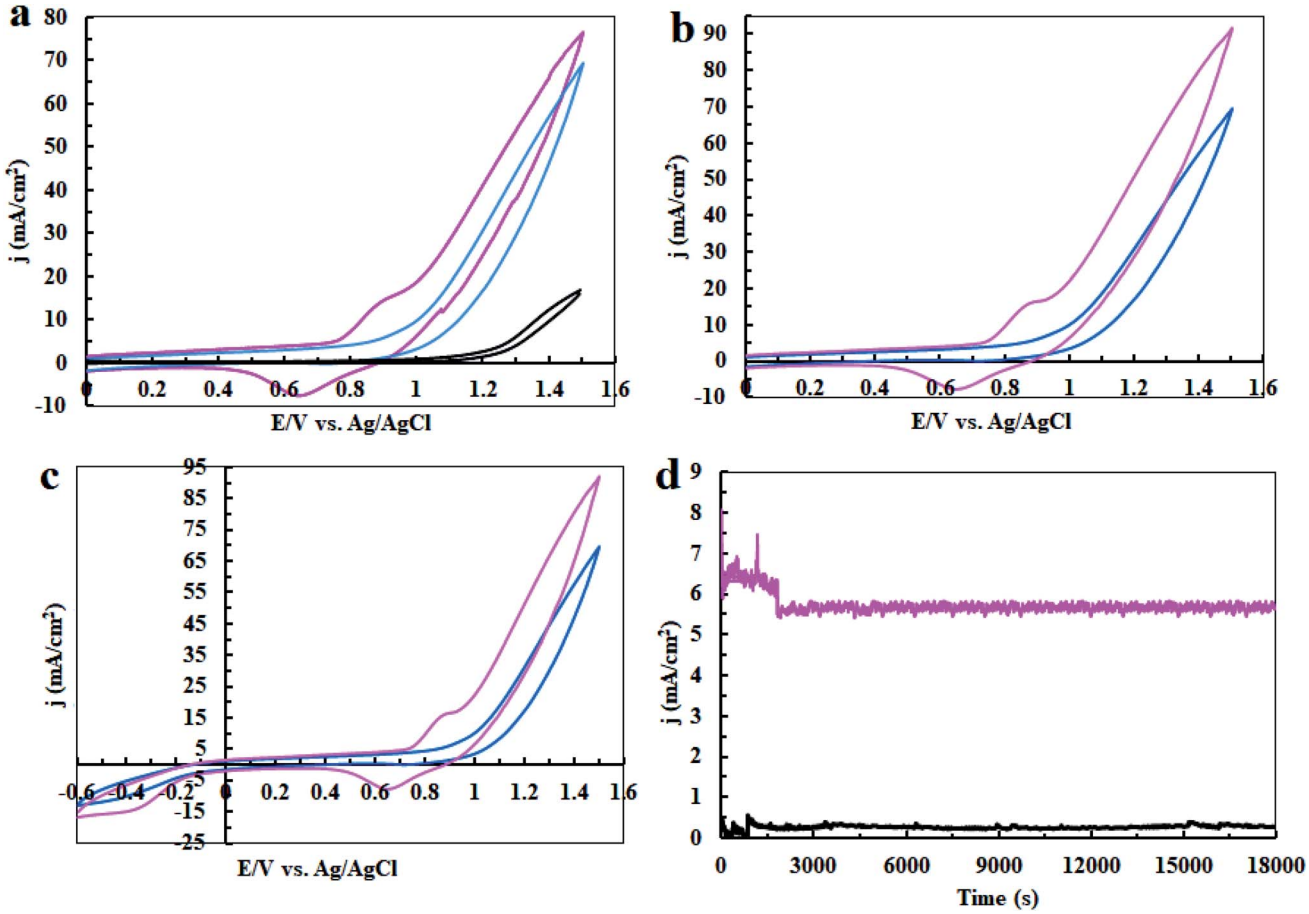

Fig. 6 Cyclic Voltammetry (CV) for a fresh CPE (black), CPE-complex **1** (blue) and CPE-complex **1** after performing amperometry of 5 hours (pink) in the buffer solution (0.5 M) in the range of 0–1.6 V (a); CV conditions: buffer solution at pH = 11 and scan rate of 50 mV s^{-1}; amperometry conditions: 1.12 V *vs.* Ag/AgCl; CPE-complex **1** in a buffer solution (25 ml) at pH = 11. The 5th and 50th CV for CPE-complex **1** (blue and pink, respectively) in 25 ml of buffer solution (0.5 M) at pH = 11 and scan rate of 50 mV s^{-1} in the range of 0 to +1.6 V *vs.* Ag/AgCl (b); and in the range of −0.6 to +1.6 V (c). Amperometry for a fresh CPE (black) and CPE-complex **1** (pink) in buffer solution; amperometry conditions: 1.12 V *vs.* Ag/AgCl: in buffer solution (25 ml) at pH = 11 (d).

redox couple of Ni(I)/Ni(II) with half wave potential of −1.38 V *vs.* Ag/AgCl. Moreover, the anodic peak at 0.445 V *vs.* Ag/AgCl and the cathodic peak at −0.791 V *vs.* Ag/AgCl can be related to the irreversible oxidation and reduction of the ligand.

In the next step, the electrocatalytic activity of complex **1** for water oxidation was tested in 0.5 M of borate buffer at pH = 3, 7 and 11 in a typical three-electrode setup with a scan rate of 50 mV s^{-1}. Fig. 5 shows the linear sweep voltammetry (LSV) curves of bare carbon paste electrode (CPE) and carbon paste electrode modified with complex **1** (CPE-complex **1**) in a borate buffer solution and at pH = 3, 7 and 11. The bare CPE shows very poor water oxidation activity with the need of large overpotential 500, 470 and 290 mV *vs.* Ag/AgCl to drive 0.7, 0.8 and 2.0 mA cm^{-2} as the selected current density in pH = 3, 7 and 11, respectively, while complex **1** shows a good activity and only demands overvoltage of 140, 35 and 21 mV *vs.* Ag/AgCl for approaching 0.7, 0.8 and 2.0 mA cm^{-2} as the selected current density under the same conditions (Fig. 5a–c). Therefore, complex **1** exhibits a much superior activity and only needs 21 mV overvoltage to reach a geometrical catalytic current density of 2.0 mA cm^{-2} at pH = 11. Also, as expected, the onset potential decreases from 1.15 V to 0.67 V with an increase of pH from 3 to 13 under constant current density of 1.0 mA cm^{-2} (Fig. 5d). Tafel plots of CPE-complex **1** electrocatalyst at pH = 3, 7 and 11 are shown in Fig. 5e. The Tafel slopes increase for complex **1** in the following order: pH = 3 > pH = 7 > pH = 11. LSV results indicate a higher current density for CPE-complex **1** in pH = 11 than the others at a certain applied potential. The current density at pH = 3 rises more rapidly with the increase in voltage. The small Tafel slope for CPE modified with complex **1** at pH = 7 and 11 shows that the electron and mass transfers on the surface of the electrode are easier than pH = 3.

In the next step, cyclic voltammetry studies were conducted at pH = 3, 7 and 11 in order to determine the true catalyst for water oxidation reaction in the presence of complex **1**. The results are presented in Fig. 6, 7, 10 and 13. As shown in Fig. 6a, the modified CPE with complex **1** is a water oxidizing catalyst in comparison to a fresh CPE at pH = 11. After carrying out the amperometry for a period of 5 hours at 1.12 V *vs.* Ag/AgCl, CPE-complex **1** becomes an efficient electrode for water oxidation.

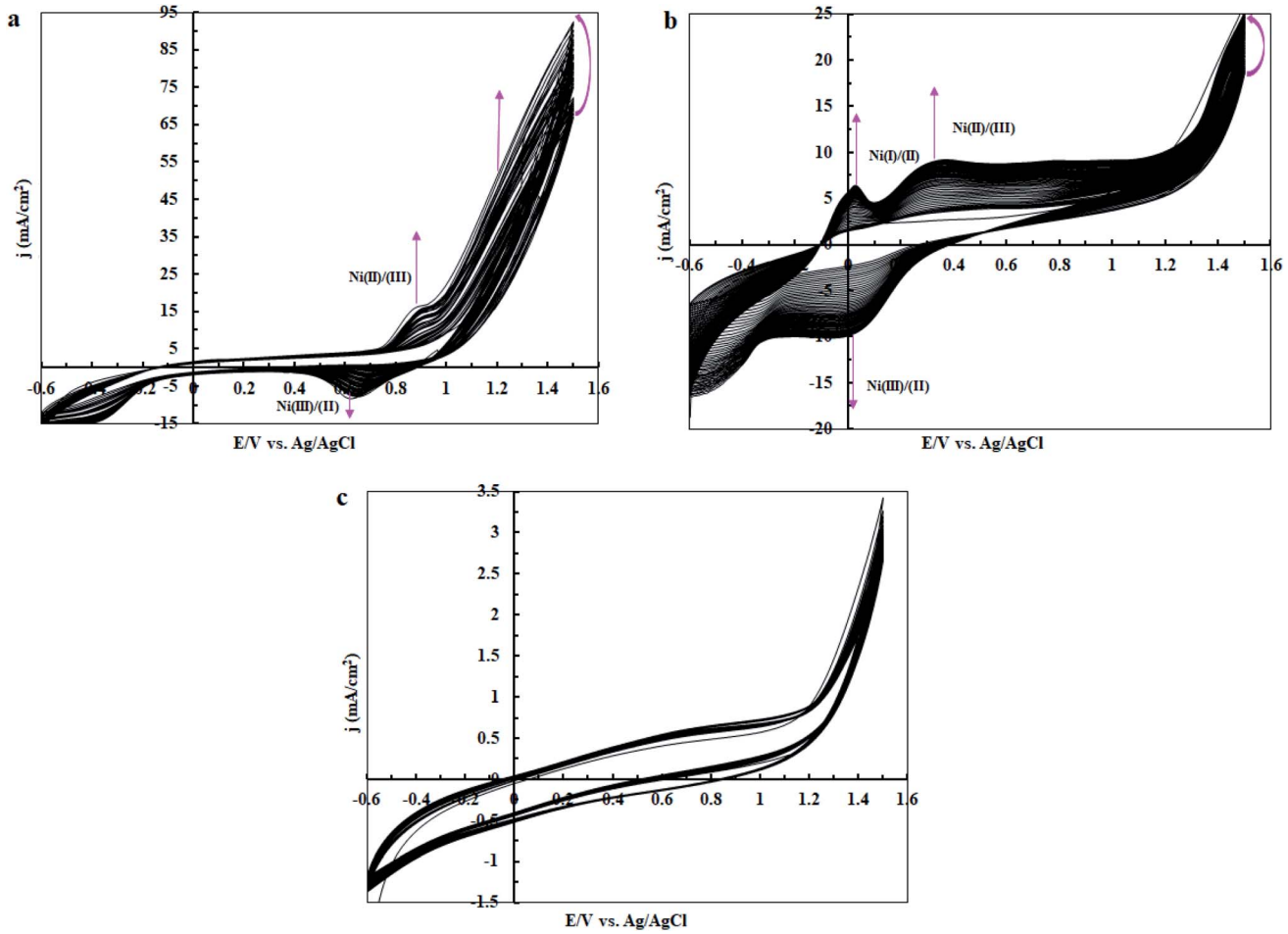

Fig. 7 Continuous CVs for CPE-complex **1** in 25 ml of borate buffer solution (0.5 M) at pH = 11 (a); pH = 7 (b); and pH = 3 (c). The scan rate in all cases is 50 mV s^{-1}.

According to the literature,[16] the increase in the efficiency of the CPE-complex **1** for oxidizing of water can be attributed to the formation of a solid on the surface of the electrode. With continuous CVs for complex **1**, two new peaks at 0.887 V and 0.633 V (*vs.* Ag/AgCl) were formed (Fig. 6b and c), which can be attributed to redox couple of Ni(II)/Ni(III).[16] The continuous CV also causes an increase in the water oxidation reaction for CPE-complex **1**. It is likely that under continues CV in the presence of complex **1**, NiO is produced which rises the oxidation of water. The amperometry (1.12 V *vs.* Ag/AgCl) for a fresh carbon paste electrode reveals low activity for water oxidation (Fig. 6d), but a CPE-complex **1** shows an increase due to Ni(II)/Ni(III) oxide formation. Then, a decrease and constant current density is observed (Fig. 6d). Finally, the continuous CVs (50 cycles) at pH = 11 for CPE-complex **1** are shown in Fig. 7a. Two peaks attributed to the oxidation of Ni(II)/Ni(III) and reduction of Ni(III)/Ni(II) are observed at 0.887 V and 0.633 V, respectively ($E_{1/2}$ = 0.76 V *vs.* Ag/AgCl and ΔE = 0.254 V) for CPE-complex **1**. Generally, the continuous CV displays a growth for Ni(II)/Ni(III) and water oxidation (Fig. 7a). According to the literature,[15,16] it seems that a significant change slowly occurs for complex **1** during the continuous CV which can be related to the deposition of material on the surface of CPE.

In the next step, the film on the surface of CPE-complex **1** was investigated by using field-emission scanning electron microscopy (FE-SEM). The results are shown in Fig. 8 and 9. The FE-SEM images clearly show the formation of NiO nanoparticles (~325–475 nm) on the surface of the electrode. The images indicate the nickel oxide nanospheres are distributed uniformly in the film on the surface of electrode (Fig. 8a). The energy dispersive X-ray analysis (EDX) reveals that the surface of CPE-complex **1** at pH = 11 consists of C, N, O, Cl, Ni and low amount of K (Fig. 8b). Also, the EDX-SEM images of the CPE-complex **1** after amperometry for 5 h reveal approximately homogenous distribution of Ni and O atoms on the electrode surface (Fig. 9). From these observations, it seems that under the present conditions a heterogeneous (NiO_x) catalyst acts as a true catalyst for the water oxidation reaction. Finally, the powder X-ray diffraction study (XRD) indicates the film is considerably amorphous which is consistent with previous studies.[16] This means that NiO on the surface of electrode does not have pure, simple and crystalline structure (Fig. S6†), but, it can be effective electrocatalyst for oxidation of water.

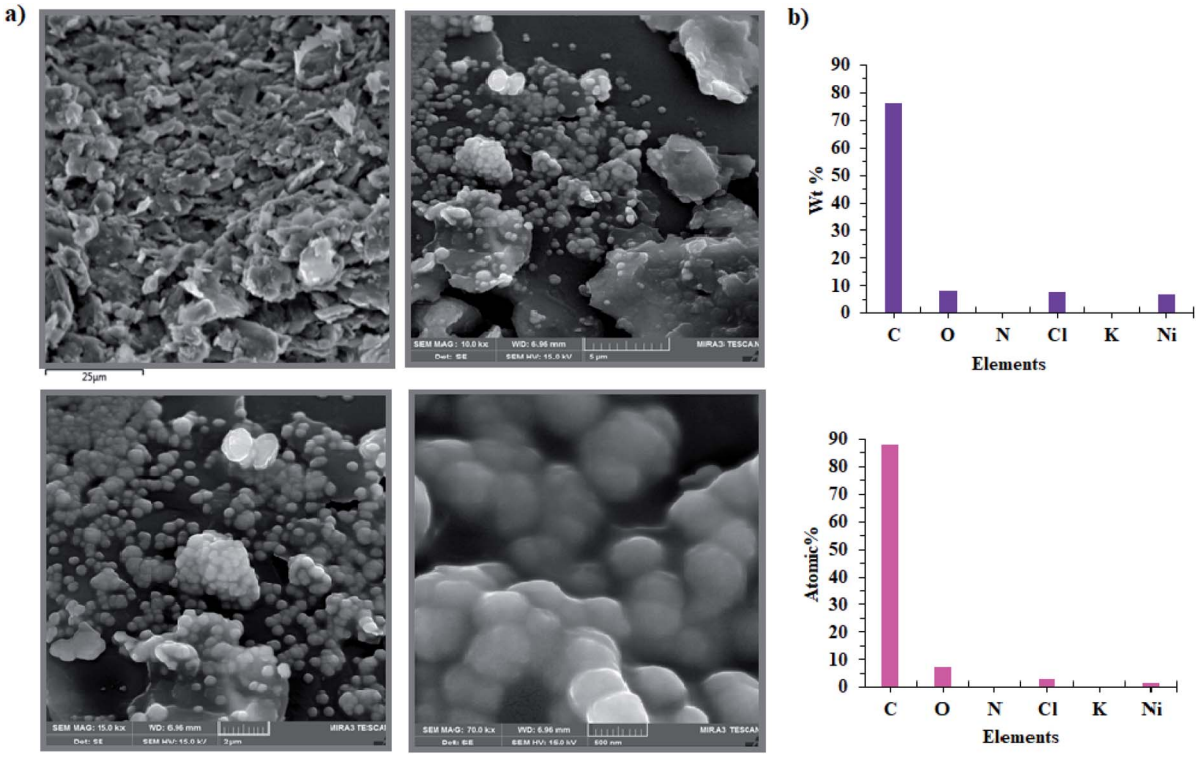

Fig. 8 FE-SEM images of CPE-complex **1** after the aerometry at 1.12 V *vs.* Ag/AgCl for 5 h under the water oxidation condition in buffer solution (pH = 11) in the bulk electrolysis of complex **1** (a) and EDX analysis for CPE-complex **1** (b).

At pH = 7, as shown in Fig. 10a and b, the designed electrode converts to an efficient catalyst for water oxidation after performing amperometry for 5 hours at 1.12 V *vs.* Ag/AgCl. This behaviour is quite similar to the observation at pH = 11. With continuous CV for complex **1**, two new anodic peaks at 0.344 and 0.0397 V (*vs.* Ag/AgCl) are formed (Fig. 10b and c), which can be attributed to the decomposition of complex **1** or Ni(II)/Ni(III) and Ni(I)/Ni(II) oxidation.[16] Surprisingly, the continuous CV also causes an increase in the water oxidation reaction for complex **1**. Therefore, we guess under CV conditions in the presence of complex **1**, NiO or other compounds of Ni are formed on the surface of the electrode which can increase the water-oxidizing activity of complex **1**. Amperometry (1.12 V) reveals sensible improvement in water oxidation in the presence of CPE-complex **1** (Fig. 10a and d). The amperometry for a fresh CPE shows a low activity for water oxidation, but the

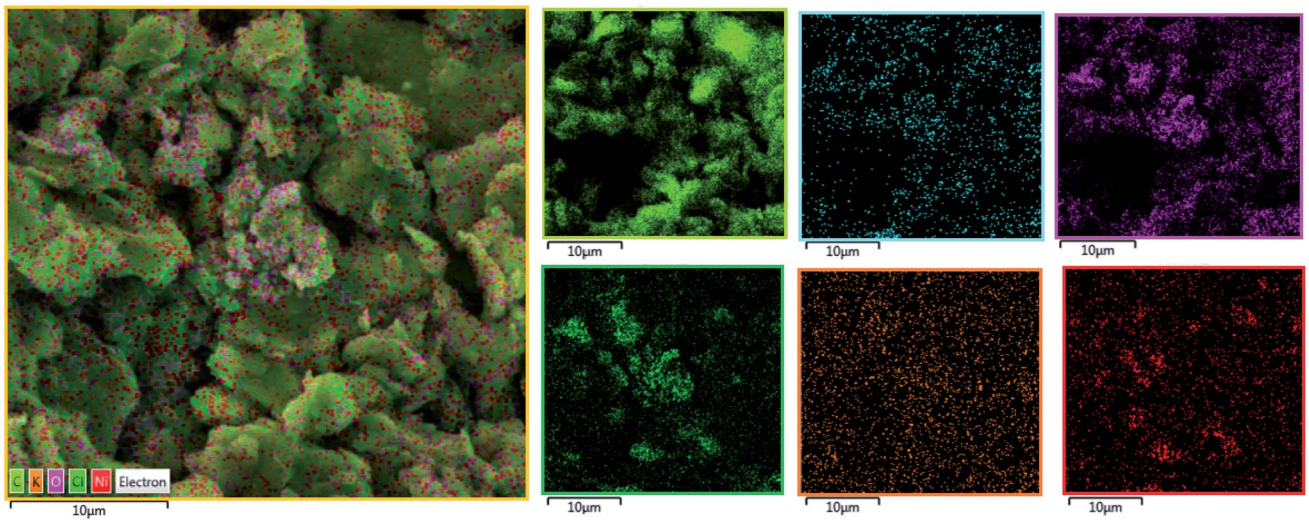

Fig. 9 EDX-SEM images of the CPE-complex **1** after the reaction (C (light green); N (blue); O (pink); Cl (dark green); K (orange); Ni (red)).

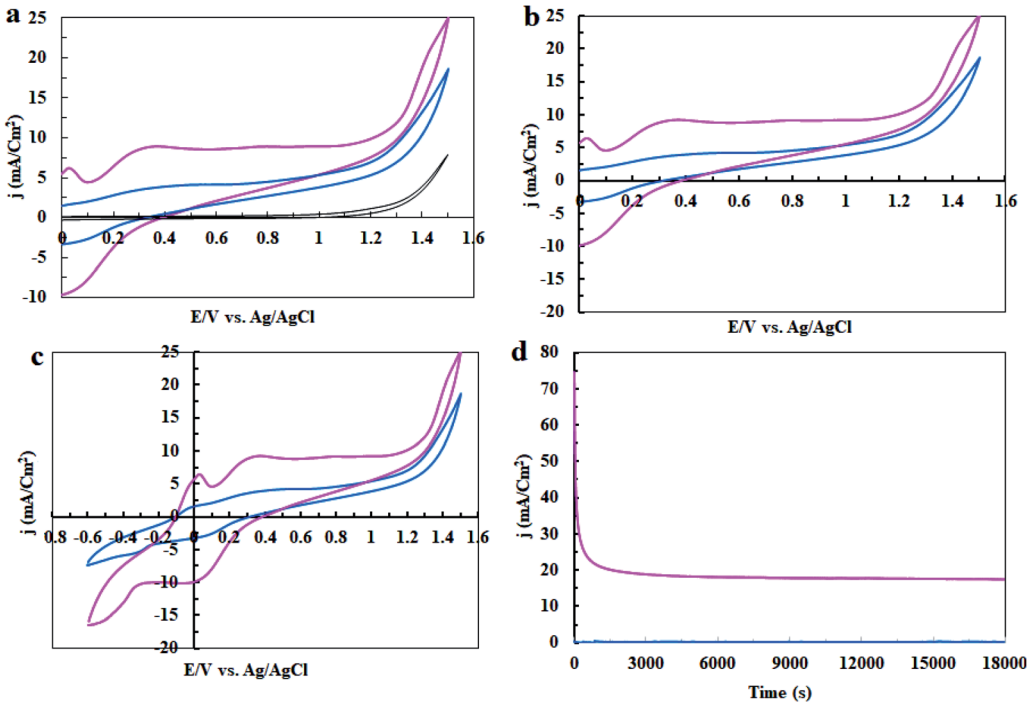

Fig. 10 CV for a fresh CPE (black), CPE-complex **1** (blue) and CPE-complex **1** after performing amperometry for 5 hours (pink) in the buffer solution (0.5 M) in the range of 0–1.6 V *vs.* Ag/AgCl (a); CV conditions: buffer solution at pH = 7 and scan rate of 50 mV s^{-1}; amperometry conditions: 1.12 V *vs.* Ag/AgCl; CPE-complex **1** in buffer solution (25 ml). The 5th and 50th CV for CPE-complex **1** (blue and pink, respectively) in 25 ml of buffer solution (0.5 M) in the range of 0 to +1.6 V *vs.* Ag/AgCl (b); and in the range of −0.6 to +1.6 V (c); CV conditions: buffer solution at pH = 7 and scan rate of 50 mV s^{-1}. Amperometry for a fresh CPE (black) and CPE-complex **1** (pink) in buffer solution (d); amperometry conditions: 1.12 V *vs.* Ag/AgCl: in buffer solution (25 ml) at pH = 7.

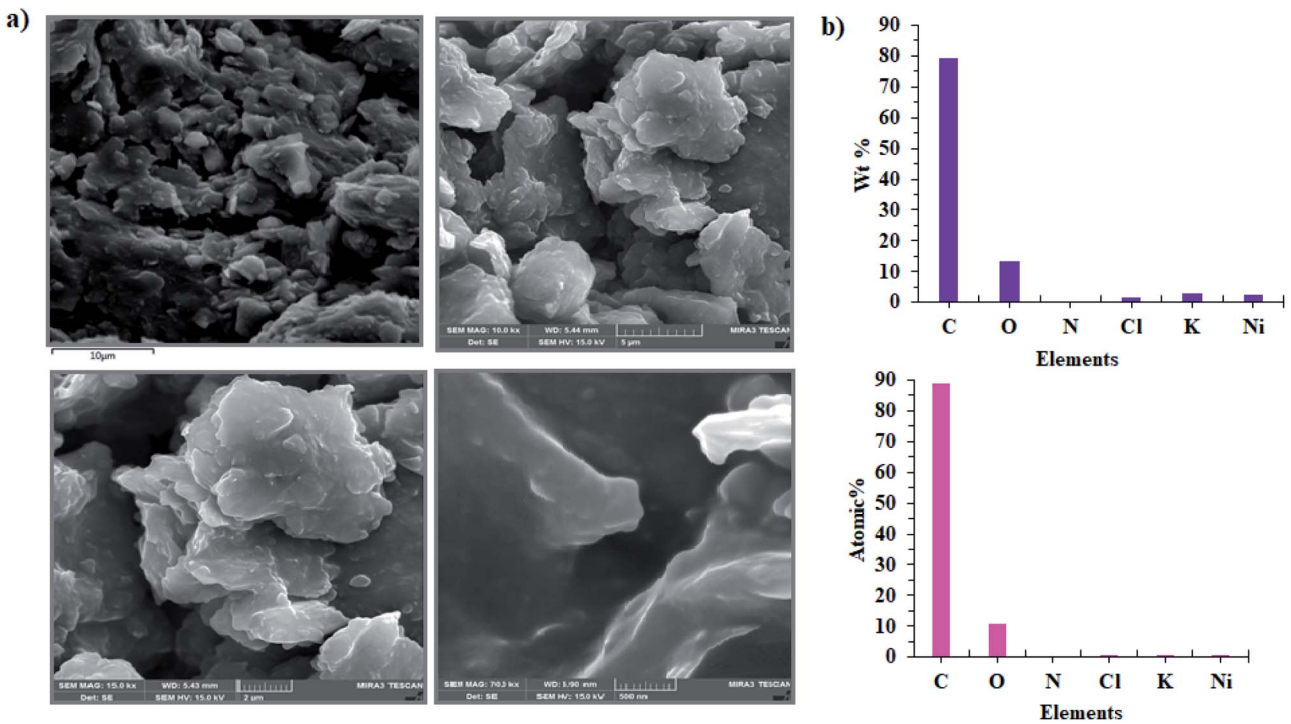

Fig. 11 FE-SEM images of CPE-complex **1** after the aerometry for 5 h under the water oxidation condition in buffer solution (pH = 7) in the bulk electrolysis of complex **1** at 1.12 V *vs.* Ag/AgCl (a) and EDX analysis for CPE-complex **1** (b).

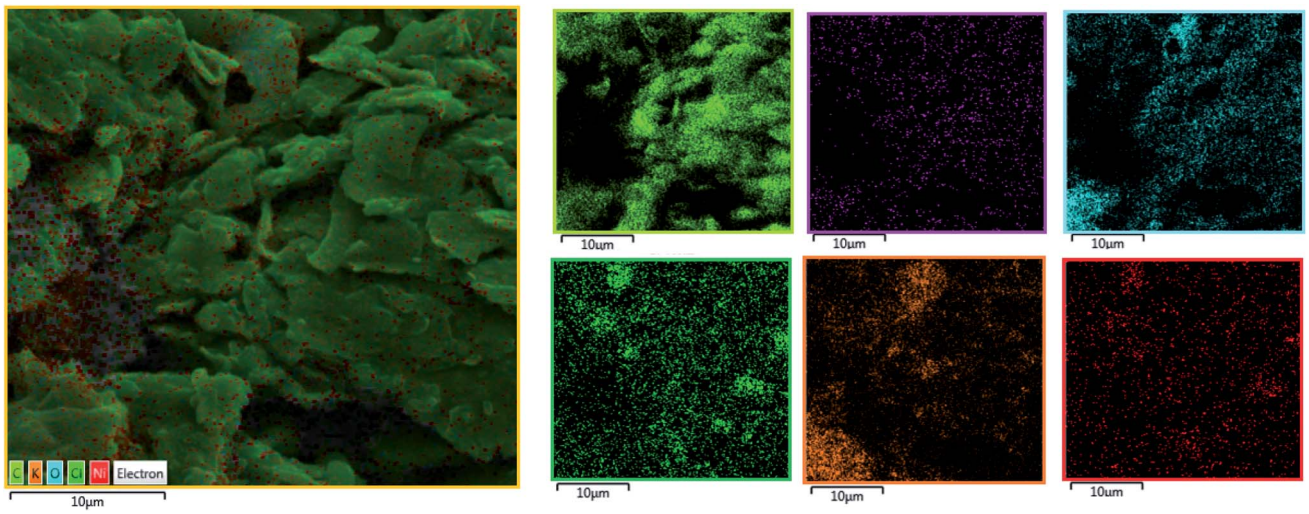

Fig. 12 EDX-SEM images of the CPE-complex **1** after the reaction (C (light green); N (violet); O (blue); Cl (dark green); K (orange); Ni (red)).

CPE-complex **1** shows a high and constant current density (Fig. 10d). The continuous CVs (50 cycles) at pH = 7 for CPE-complex **1** are shown in Fig. 7b. For complex **1**, the continuous CV displays an increase in the attributed peaks to the redox couple of Ni(II)/Ni(III) and oxidation of Ni(I)/(II) at 0.344, 0.0299 and 0.0397 V *vs.* Ag/AgCl, respectively, which

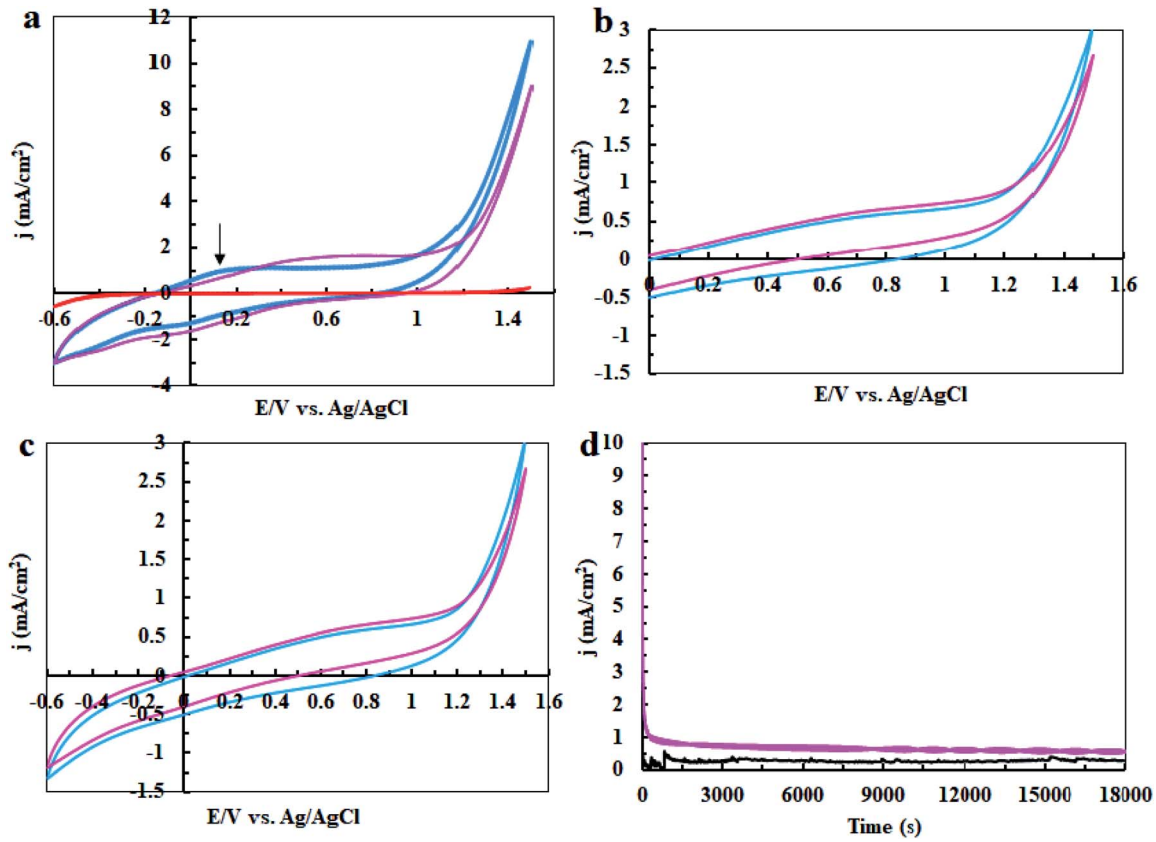

Fig. 13 CV for a fresh CPE (black), CPE-complex **1** (blue) and CPE-complex **1** after performing amperometry for 5 hours (pink) in the buffer solution (0.5 M) in the range of −0.6 to +1.6 V *vs.* Ag/AgCl (a); CV conditions: buffer solution at pH = 3 and scan rate of 50 mV s^{-1}; amperometry conditions: 1.12 V *vs.* Ag/AgCl. The 5th and 50th CV for CPE-complex **1** (blue and pink, respectively) in 25 ml of buffer solution (0.3 M) at pH = 3 and scan rate of 50 mV s^{-1} in the range of 0 to +1.6 V (b); and in the range of −0.6 to +1.6 V (c). Amperometry for a fresh CPE (black) and CPE-complex **1** (pink) in buffer solution; amperometry conditions: 1.12 V *vs.* Ag/AgCl: in buffer solution (25 ml) at pH = 3 (d).

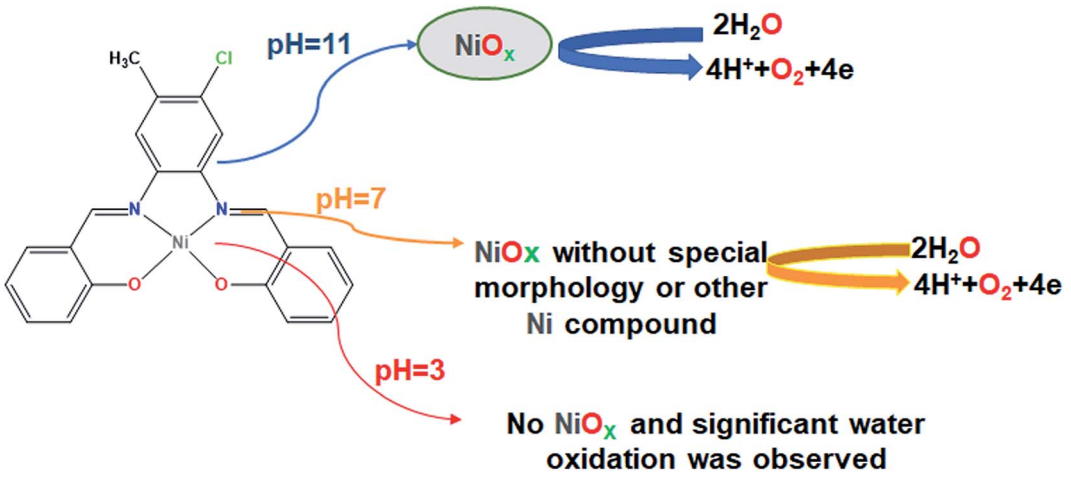

Fig. 14 A simple scheme of suggested mechanism for water oxidation reaction in the presence of complex **1** in different pH.

Table 2 Crystallographic data and refinement details for complex **1**

Compound	Complex **1**
Formula	$C_{21}H_{15}ClN_2NiO_2$
M_r/g mol^{-1}	421.51
Crystal shape, color	Needle, red
Crystal size/mm^3	0.19 × 0.08 × 0.02
Crystal system	Monoclinic
Space group	$P2_1/c$
a/Å	11.0230(14)
b/Å	8.0024(8)
c/Å	19.532(2)
β/°	106.302(12)
V Å^{-3}	1653.6(3)
Z	4
D_{calc}/g cm^{-3}	1.693
μ/mm^{-1}	1.36
F(000)	864
θ range/°	1.9–28.4
h, k, l	−14 → 14
	−10 → 8
	−18 → 26
Measured reflections	12 101
Independent reflections	3825
Reflections with $I > 2\sigma(I)$	1214
R_{int}	0.215
$R[F^2 > 2\sigma(F^2)]$	0.094
w$R(F^2)$	0.346
S	0.99
Abs. correction	Analytical
Parameters	246
Restraints	0
$\Delta\rho_{max}/\Delta\rho_{min}$	0.53/−0.59

indicates that the complex is stable under these conditions. Anyway, in this condition the current density for water oxidation increases slightly in comparison with pH = 11 (Fig. 7a and b). This is not surprising because, in contrast to that of pH = 11, the nanosized NiO is relatively soluble at pH = 7.

Our findings are surprising since the designed Ni(II) salophen complex can show high efficiency for water oxidation under applied electrochemical conditions at neutral solution as well as alkaline condition, while the Ni-salen complex (with the non-aromatic ligand) that was previously investigated by Najafpour *et al.*[16], only revealed good electrocatalytic activity for water oxidation at pH = 11 and was not stable in neutral solution and showed low activity for water oxidation.[16] This may be due to the effect of the aromatic ligand compared to its non-aromatic counterpart. Finally, the surface of the CPE-complex **1** is studied by FE-SEM images after the amperometry (Fig. 11a). The SEM images show no a special new morphology, but the EDX data from the surface of the electrode show low amounts of Ni which Ni is dispersed on the surface of the electrode (Fig. 11b).[15] Although, compared to pH = 11, the formation of nickel oxide nanoparticles with the spherical morphology on the electrode surface is not clearly observed and in addition the amount of nickel on the surface of the electrode is low and also the nature of the Ni compound on CPE is not exactly known. But, it shows a high catalytic performance for water oxidation reaction. More interestingly, unlike that observed at pH = 11, Ni and O atoms are uniformly distributed on the electrode surface (Fig. 12). Consequently, we guess that a heterogeneous Ni-based compound catalyzes water oxidation reaction under the electrochemical conditions.

Finally, we studied the water oxidation activity of complex **1** in a buffer solution at pH = 3. As shown in Fig. 13a–d, CV and amperometry display no efficient water-oxidizing activity for complex **1** under these conditions. In the CV of fresh CPE-complex **1**, one peak in the 0.20 V *vs.* Ag/AgCl is observed which can be attributed to the decomposition of complex **1** and Ni(II)/Ni(III) oxidation (Fig. 13a). This peak is not observed during continuous CV (Fig. 13b and c). This indicates that complex **1** is not stable under these conditions. During amperometry, complex **1** does not show water oxidation activity and only a low current density is observed (Fig. 13d). This can be related to the high solubility of NiO at pH = 3. Also, the continuous CVs (50 cycles) for complex **1** at pH = 3 are given in Fig. 7c which indicates the attributed peak for the complex disappears in this condition. This observation confirms that the

complex is not stable under these conditions and no significant water oxidation was observed (Fig. 14).

Conclusions

The design of efficient electrocatalysts for water splitting as a clean and renewable energy resource in recent years has been of a great interest. For this purpose, a new mononuclear Ni(II) salophen-type complex was synthesized by the reaction of a salophen-type N_2O_2-donor ligand and $Ni(OAc)_2 \cdot 4H_2O$ and was characterized by spectroscopic methods and single crystal X-ray analysis. The water-oxidizing activity of the obtained complex was studied at three different pH (pH = 3, 7 and 11). LSV curves showed that the CPE modified with complex **1** can exhibit a high electrocatalytic activity for the oxidizing of water in basic and neutral solutions in terms of the onset potential and Tafel slope. Also, cyclic voltammetry experiments and FE-SEM images showed that at pH = 11, NiO_x is the heterogeneous catalyst for water oxidation under electrochemical water oxidation conditions and in the presence of complex **1**. Surprisingly, our experiments showed that complex **1** can also act as an efficient electrocatalyst for water oxidation at pH = 7. FE-SEM images did not clearly show the formation of NiO on the surface of the electrode (and also a special new morphology), but the EDX data from the surface of CPE showed a low amount of Ni. Although the nature of the Ni compound on the electrode surface was not clear, but it could show a high catalytic performance for water oxidation reaction. Finally, at pH = 3, no significant water oxidation was observed.

Experimental section

Materials and instrumentation

4-Chloro-5-metyl-1,2-diaminobenzene, 2-hydroxybenzaldehyde and Ni(II) acetate tetrahydrate were purchased from Sigma-Aldrich company. Solvents with highest purity were provided from Merck and used without further purification. Graphite powder and paraffin oil from Merck were used for the preparation of carbon paste electrode. To adjust the pH of the electrolyte solution at pH = 3–11, 0.5 M of boric acid, 1.0 M of HCl and 1.0 M of NaOH solutions were used. NMR spectra were recorded on a Bruker Avance DPX-400 MHz spectrometer. The elemental analyses (carbon, hydrogen and nitrogen) of the compounds were obtained from a Carlo ERBA Model EA 1108 analyzer. FT-IR spectra were prepared with a FT-IR Spectrometer Bruker Tensor 27 after mixing the samples with KBr. Electronic absorption spectra were obtained with T 60 UV/Vis Spectrometer PG Instruments Ltd. X-ray diffraction patterns of electrodes were obtained using Bruker AXS model D8-Advance diffractometer equipped with Cu-K_α radiation at $\lambda = 1.5418$ Å from $2\theta = 30^\circ$ to 70°. Surface morphology of electrodes was studied using TESCAN mira 3 field-emission scanning electron microscope (FE-SEM) equipped with energy dispersive X-ray analysis (EDX).

Synthesis of 2,2′-((1*E*,1′*E*)-((4-chloro-5-methyl-1,2-phenylene) bis(azanylylidene))bis(methanylylidene))diphenol (H_2L)

4-Chloro-5-metyl-1,2-diaminobenzene (1.00 g, 6.38 mmol) in 30 ml ethanol was slowly added to ethanol solution of salicylaldehyde (1.36 ml, 12.76 mmol) under stirring in room temperature. Immediately, the color of the solution turned to orange-brown and precipitate was appeared after a few minutes. The reaction was continued for 4 h at room temperature (the end of the reaction was controlled by thin layer chromatography (TLC)). The precipitate was filtered, washed with ethanol and dried at air. Yield: 84.2% (1.96 g). Anal. calc. for $C_{21}H_{17}N_2O_2Cl$ ($M = 364.82$): C, 69.14; H, 4.70; N, 7.68%. Found: C, 69.19; H, 4.67; N, 7.61%. ^{1}H NMR (400 MHz, DMSO-d_6): δ 12.77 (s, 1H, –OH), 12.69 (s, 1H, –OH), 8.99 (s, 1H, –HC=N–), 8.95 (s, 1H, –HC=N–), 7.70 (s, 1H, Ar–H), 7.60 (s, 1H, Ar–H), 7.49 (d, 2H, J = 8.8 Hz, ArH), 7.45–7.42 (m, 2H, ArH), 7.02–6.97 (m, 4H, ArH), 2.34 (s, 3H, $-CH_3$); FT-IR (KBr, cm^{-1}): 3447 (b),1614 (*vs.*), 1578 (m), 1478 (s), 1558 (m), 1405 (m), 1276 (s), 1224 (w), 1190 (m), 1151 (m), 1115 (m), 1085 (s), 969 (m), 920 (w), 907 (w), 893 (m), 866 (w), 811 (m), 752 (s), 697 (w), 652 (w), 591 (w), 503 (w), 437 (w).

Synthesis of complex 1

Complex **1** was synthesized by the reaction of H_2L (0.100 g, 0.274 mmol) and $Ni(OAc)_2 \cdot 4H_2O$ (0.068 g, 0.274 mmol) in ethanol by using a branched tube. Mentioned amounts of materials were placed in the main arm of a branched tube. Ethanol was carefully added to fill the arms. The tube was tight closed and the arm containing the reagents was immersed in an oil bath at 70 °C, while the other arm was kept at ambient temperature. After four days, red crystals were formed in the cooler arm. The crystals were filtered off, washed with ethanol and dried at air. Yield: 74% (0.085 g). Anal. calc. for $C_{21}H_{15}N_2NiO_2Cl$ ($M_w = 421.51$ g mol^{-1}): C, 59.84; H, 3.59; N, 6.65; Ni, 13.92%. Found: C, 59.89; H, 3.62; N, 6.61; Ni, 13.85%. ^{1}H NMR (400 MHz, DMSO-d_6): δ 9.02 (s, 1H, –HC=N–), 8.97 (s, 1H, –HC=N–), 8.32 (s, 1H, ArH), 8.19 (d, 1H, J = 8.8 Hz, ArH), 7.60 (d, 2H, J = 7.62, Ar–H), 7.34–7.36 (m, 2H, Ar–H), 6.92 (d, 2H, J = 8.4 Hz, ArH), 6.68–6.73 (m, 2H, ArH), 2.15 (s, 3H, $-CH_3$). FT-IR (KBr, cm^{-1}): 3420 (m, br), 1608 (s), 1574 (s), 1522 (m), 1488 (m), 1460 (m), 1441 (m), 1368 (m), 1333 (m), 1262 (s), 1231 (m), 1196 (m), 1149 (m), 1132 (m), 1090 (m), 1022 (m), 1057 (m), 946 (w), 900 (w), 846 (m), 799 (w), 752 (s), 709 (w), 595 (w), 556 (w), 449 (w).

Single crystal X-ray analysis

The molecular structure of complex **1** was determined by single crystal X-ray analysis at 293(2) K. The data collection was performed on an Oxford Sapphire CCD diffractometer using Mo Kα radiation ($\lambda = 0.71073$ Å) and ω–2θ method. The structure was solved by direct methods and refined with the full-matrix least-squares method on F^2 with the use of SHELX-2014 program packages.[32] The analytical absorption corrections were applied.[33] Positions of hydrogen atoms have been found from the electron density maps and hydrogen atoms were

constrained during refinement with the appropriate riding model as implemented in SHELX during refinement. A summary of the crystal data and refinement details for complex **1** is given in Table 2. The structural data have been deposited at the Cambridge Crystallographic Data Centre: (CCDC no. 1954803).†

Electrochemical tests

Electrochemical analyses of complex **1** were done by using an Autolab PGSTAT204. The carbon paste electrode (CPE) modified with complex **1** was used as working electrode. The Ag/AgCl and Pt wire electrodes were used as reference and counter electrodes, respectively. CPE modified with complex **1** (CPE-complex **1**) was fabricated as follows: graphite powder, complex **1** and paraffin oil with a mass ratio of 80 : 15 : 5 were mixed using a mortar until a homogenous paste was obtained. Then, the obtained homogenous paste was packed in a copper wire with a 1.10 mm radius. The unmodified CPE electrode was fabricated using the same method. The surface of CPE electrodes was smoothed and the electrodes were washed with double distilled water.[34]

Conflicts of interest

There are no conflicts to declare.

Acknowledgements

The authors are grateful to Azarbaijan Shahid Madani University, Imam Khomeini International University and Nicolaus Copernicus University in Torun for financial support of this study.

References

1 R. Esinberg and D. G. Nocera, *Inorg. Chem.*, 2005, **44**, 6799–6801.

2 (*a*) Y. Gao, H. Chen, L. Ye, Z. Lu, Y. Yao, Y. Wei and X. Chen, *Chin. J. Catal.*, 2018, **39**, 479–486; (*b*) A. Han, H. Jia, H. Ma, S. Ye, H. Wu, H. Lei, Y. Han, R. Cao and P. Du, *Phys. Chem. Chem. Phys.*, 2014, **16**, 11209–11217; (*c*) M. Yagi and M. Kaneko, *Chem. Rev.*, 2001, **101**, 21–36; (*d*) W. Rüttinger and G. C. Dismukes, *Chem. Rev.*, 1997, **97**, 1–24; (*e*) G. Liao, Y. Gong, L. Zhang, H. Gao, G.-J. Yang and B. Fang, *Energy Environ. Sci.*, 2019, **12**, 2080–2147; (*f*) W. Zhong, Z. Lin, S. Feng, D. Wang, S. Shen, Q. Zhang, L. Gu, Z. Wang and B. Fang, *Nanoscale*, 2019, **11**, 4407–4413; (*g*) D. Wang, D. Zhang, C. Tang, P. Zhou, Z. Wu and B. Fang, *Catal. Sci. Technol.*, 2016, **6**, 1952–1956; (*h*) W. Zhong, S. Shen, M. He, D. Wang, Z. Wang, Z. Lin, W. Tu and J. Yu, *Appl. Catal. B Environ.*, 2019, **258**, 117967; (*i*) Y. Zhang, X. Wang, F. Luo, Y. Tan, L. Zeng, B. Fang and A. Liu, *Appl. Catal. B Environ.*, 2019, **256**, 117852; (*j*) Z. Wu, B. Fang, A. Bonakdarpour, A. Sun, D. P. Wilkinson and D. Wang, *Appl. Catal. B Environ.*, 2012, **125**, 59–66; (*k*) W. Zhong, W. Tu, S. Feng and A. Xu, *J. Alloys Compd.*, 2019, **772**, 669–674.

3 M. A. Asraf, H. A. Younus, M. Yusubov and F. Verpoort, *Catal. Sci. Technol.*, 2015, **5**, 4901–4925.

4 J. Lin, B. Ma, M. Chen and Y. Ding, *Chin. J. Catal.*, 2018, **39**, 463–471.

5 (*a*) M. M. Najafpour, S. Mehrabani, Y. Mousazade and M. Holynska, *Dalton Trans.*, 2018, **47**, 9021–9029; (*b*) J. P. McEvoy and G. W. Brudvig, *Chem. Rev.*, 2006, **106**, 4455–4483; (*c*) M. D. Karkas, O. Verho, E. V. Johnston and B. Ekermark, *Chem. Rev.*, 2014, **114**, 11863–12001; (*d*) J. Limburg, J. S. Vrettos, L. M. Liable-Sands, A. L. Rheingold, R. H. Crabtree and G. W. Brudvig, *Science*, 1999, **283**, 1524–1527; (*e*) W. J. Youngblood, S.-H. A. Lee, Y. Kobayashi, E. A. Hernandez-Pagan, P. G. Hoertz, T. A. Moore, A. L. Moore, D. Gust and T. E. Mallouk, *J. Am. Chem. Soc.*, 2009, **131**, 926–927; (*f*) T. W. Kim and K.-S. Choi, *Science*, 2014, **343**, 990–994.

6 P. Du and R. Eisenberg, *Energy Environ. Sci.*, 2012, **5**, 6012–6021.

7 (*a*) M. Wiechen, M. M. Najafpour, S. Allakhverdiev and L. Spiccia, *Energy Environ. Sci.*, 2014, **7**, 2203–2212; (*b*) M. M. Najafpour, G. Renger, M. Hołyńska, A. N. Moghaddam, E.-M. Aro, R. Carpentier, H. Nishihara, J. J. Eaton-Rye, J.-R. Shen and S. I. Allakhverdiev, *Chem. Rev.*, 2016, **116**, 2886–2936; (*c*) W. M. C. Sameera, C. J. McKenzie and J. E. McGrady, *Dalton Trans.*, 2011, **40**, 3859–3870; (*d*) R. Brimblecombe, A. Koo, G. C. Dismukes, G. F. Swiegers and L. Spiccia, *J. Am. Chem. Soc.*, 2010, **132**, 2892–2894.

8 (*a*) J. L. Fillol, Z. Codola, I. Garcia-Bosch, L. Gomez, J. J. Pla and M. Costas, *Nat. Chem.*, 2011, **3**, 807–813; (*b*) D. Hong, S. Mandal, Y. Yamada, Y.-M. Lee, W. Nam, A. Llobet and S. Fukuzumi, *Inorg. Chem.*, 2013, **52**, 9522–9531; (*c*) W.-P. To, T. W.-S. Chow, C.-W. Tse, X. Guan, J.-S. Huang and C.-M. Che, *Chem. Sci.*, 2015, **6**, 5891–5903; (*d*) V. K. K. Praneeth, M. Kondo, M. Okamura, T. Akai, H. Izu and S. Masaoka, *Chem. Sci.*, 2019, **10**, 4628–4639.

9 (*a*) A. Singh, S. L. Y. Chang, R. K. Hocking, U. Bach and L. Spiccia, *Catal. Sci. Technol.*, 2013, **3**, 1725–1732; (*b*) G. Chen, L. J. Chen, S. W. Ng and T. C. Lau, *ChemSusChem*, 2014, **7**, 127–134.

10 (*a*) M. M. Najafpour and H. Feizi, *Catal. Sci. Technol.*, 2018, **8**, 1840–1848; (*b*) T. T. Li, J. Qian, Q. Zhou, J. L. Lin and Y. Q. Zheng, *Dalton Trans.*, 2017, **46**, 13020–13026; (*c*) B. Huang, Y. Wang, S. Zhan and J. Ye, *Appl. Surf. Sci.*, 2018, **396**, 121–128; (*d*) H. Chen, Z. Sun, X. Liu, A. Han and P. Du, *J. Phys. Chem. C*, 2015, **119**, 8998–9004; (*e*) H. T. Shi, X. X. Li, F. H. Wu and W. B. Yu, *Dalton Trans.*, 2017, **46**, 16321–16326.

11 (*a*) M.-T. Zhang, Z. Chen, P. Kang and T. J. Meyer, *J. Am. Chem. Soc.*, 2013, **135**, 2048–2051; (*b*) S. M. Barnett, K. I. Goldberg and J. M. Mayer, *Nat. Chem.*, 2012, **4**, 498–502; (*c*) F. Yu, F. Li, J. Hu, L. Bai, Y. Zhu and L. Sun, *Chem. Commun.*, 2016, **52**, 10377–10380; (*d*) P. Garrido-Barros, I. Funes-Ardoiz, S. Drouet, J. Benet-Buchholz, F. Maseras and A. Llobet, *J. Am. Chem. Soc.*, 2015, **137**, 6758–6761.

12 K. Kinoshita, *Electrochemical Oxygen Technology*, Wiley-Interscience, New York, 1992.

13 (*a*) M. Gao, W. Sheng, Z. Zhuang, Q. Fang, S. Gu, J. Jiang and Y. Yan, *J. Am. Chem. Soc.*, 2014, **136**, 7077–7084; (*b*) M. Gong, W. Zhou, M. C. Tsai, J. Zhou, M. Guan, M. C. Lin, B. Zhang, Y. Hu, D. Y. Wang, J. Yang, S. J. Pennycook, B. J. Hwang and H. Dai, *Nat. Commun.*, 2014, **5**, 7077–7084; (*c*) K. Sun, N. Park, Z. Sun, J. Zhou, J. Wang, X. Pang, S. Shen, S. Y. Noh, Y. Jing, S. Jin, P. K. L. Yu and D. Wang, *Energy Environ. Sci.*, 2012, **5**, 7872–7877; (*d*) X. Yu, P. Xu, T. Hua, A. Han, X. Liu, H. Wu and P. Du, *Int. J. Hydrogen Energy*, 2014, **39**, 10467–10475.

14 J. Lin, P. Kang, X. Liang, B. Ma and Y. Ding, *Electrochim. Acta*, 2017, **258**, 353–359.

15 G. Azadi, Z. Zand, Y. Mousazade, R. Bagheri, J. Cui, Z. Song, R. Bikas, K. Wozniak, S. I. Allakhverdiev and M. M. Najafpour, *Int. J. Hydrogen Energy*, 2019, **44**, 2857–2867.

16 H. Feizi, F. Shiri, R. Bagheri, J. P. Singh, K. H. Chae, Z. Song and M. M. Najafpour, *Catal. Sci. Technol.*, 2018, **8**, 3954–3968.

17 M. Zhang, M.-T. Zhang, C. Hou, Z.-F. Ke and T.-B. Lu, *Angew. Chem. Int. Ed.*, 2014, **53**, 13042–13048.

18 P. Garrido-Barros, S. Grau, S. Drouet, J. Benet-Buchholz, C. Gimbert-Surinach and A. Llobet, *ACS Catal.*, 2019, **9**, 3936–3945.

19 Y. Han, Y. Wu, W. Lai and R. Cao, *Inorg. Chem.*, 2015, **54**, 5604–5613.

20 L. Wang, L. Duan, R. B. Ambre, Q. Daniel, H. Chen, J. Sun, B. Das, A. Thapper, J. Uhlig, P. Dinér and L. Sun, *J. Catal.*, 2016, **335**, 72–78.

21 G. Zhu, E. N. Glass, C. Zhao, H. Lv, J. W. Vickers, Y. V. Geletii, D. G. Musaev, J. Songa and C. L. Hill, *Dalton Trans.*, 2012, **41**, 13043–13049.

22 (*a*) J. Ping, Y. Wang, Q. Lu, B. Chen, J. Chen, Y. Huang, Q. Ma, C. Tan, J. Yang, X. Cao, Z. Wang, J. Wu, Y. Ying and H. Zhang, *Adv. Mater.*, 2016, **28**, 7640–7645; (*b*) S. Nayak, L. Mohapatra and K. Parida, *J. Mater. Chem. A*, 2015, **3**, 18622–18635; (*c*) G. Y. Luo, H. H. Huang, J. W. Wang and T. B. Lu, *ChemSusChem*, 2016, **9**, 485–491; (*d*) M. M. Najafpour and H. Feizi, *Dalton Trans.*, 2012, **41**, 10292–10297.

23 (*a*) A. Singh, S. L. Y. Chang, R. K. Hocking, U. Bachcde and L. Spiccia, *Energy Environ. Sci.*, 2013, **6**, 579–586; (*b*) I. M. Sadiek, A. M. Mohammad, M. E. Shakre and M. S. Deab, *Int. J. Hydrogen Energy*, 2012, **37**, 68–77; (*c*) X. Wang, H. Luo, H. Yang, P. J. Sebastian and S. A. Gamboa, *Int. J. Hydrogen Energy*, 2004, **29**, 967–972; (*d*) M. Dinca, Y. Surendranath and D. G. Nocera, *Proc. Natl. Acad. Sci. U.S.A.*, 2010, **107**, 10337–10341.

24 L.-H. Zhang, F. Yu, Y. Shi, F. Li and H. Li, *Chem. Commun.*, 2019, **55**, 6122–6125.

25 (*a*) P. Mahapatra, M. G. B. Drew and A. Ghosh, *Dalton Trans.*, 2018, **47**, 13957–13971; (*b*) R. Bikas, E. Shahmoradi, S. Reinoso, M. Emami, L. Lezama, J. Sanchiz and N. Noshiranzadeh, *Dalton Trans.*, 2019, **48**, 13799–13812; (*c*) R. Bikas, M. Emami, K. Ślepokura and N. Noshiranzadeh, *New J. Chem.*, 2017, **41**, 9710–9717.

26 (*a*) S. Roy, A. Bhattacharyya, S. Purkait, A. Bauzá, A. Frontera and S. Chattopadhyay, *Dalton Trans.*, 2016, **45**, 15048–15059; (*b*) R. Bikas, V. Kuncser, J. Sanchiz, G. Schinteie, M. Siczek, H. Hosseini-Monfared and T. Lis, *Polyhedron*, 2018, **147**, 142–151.

27 S. Demir, H. Yılmaz, M. Dilimulati and M. Andac, *Spectrochim. Acta, Part A*, 2015, **150**, 523–532.

28 (*a*) K.-L. Kuo, C.-C. Huang and Y.-C. Lin, *Dalton Trans.*, 2008, 3889–3898; (*b*) R. Bikas, V. Lippolis, N. Noshiranzadeh, H. Farzaneh-Bonab, A. J. Blake, M. Siczek, H. Hosseini-Monfared and T. Lis, *Eur. J. Inorg. Chem.*, 2017, 999–1006.

29 L. Rigamonti, A. Forni, S. Righetto and A. Pasinic, *Dalton Trans.*, 2019, **48**, 11217–11234.

30 R. Atkins, G. Brewer, E. Kokot, G. M. Mockler and E. Sinn, *Inorg. Chem.*, 1985, **24**, 127–134.

31 (*a*) C. Gosden, K. P. Healy and D. Pletcher, *J. Chem. Soc., Dalton Trans.*, 1978, 972–976; (*b*) P. Zanello, *Inorganic electrochemistry: theory, practice and application*, Royal Society of Chemistry, 2007.

32 G. M. Sheldrick, *Acta Crystallogr.*, 2015, **71**, 3–8.

33 *CrysAlis 171.38.43 package of programs*, Rigaku Oxford Diffraction, 2015.

34 L. J. Foruzin, B. Habibi and Z. Rezvani, *New J. Chem.*, 2018, **42**, 13963–13970.

